Nuclear dynamics in a positron-CO collision using close-coupling methods

T. Mukherjee*
Department of Physics, Bhairab Ganguly College, Kolkata-700056, India
(Received 7 August 2017; published 17 October 2017)

Apart from the electronic motion of the target in the molecular collision process, collision probabilities strongly depend on the dynamics of nuclear motions (rotation and vibration). Here we have studied this nuclear dynamical dependency of collision cross sections for a positron–carbon monoxide collision using rovibrational close-coupling, rotational laboratory frame close-coupling (rotational LFCC), and LFCC adiabatic nuclear vibration (LFCC-ANV) methods. Here we have computed the angle-integrated elastic and state-to-state rotational excitation, the elastic and state-to-state vibrational (summed over rotational) excitation, and the total (summed over rotational and vibrational) cross sections for the incident positron energy between 0.0 and 7.0 eV using the rovibrational close-coupling method. The rotational LFCC method is also employed to calculate elastic, (state-to-state) rotational excitation, and total cross sections. To estimate the effects of the nuclear dynamics we have calculated vibrational elastic and state-to-state vibrational excitation cross sections using the LFCC-ANV method. In these calculations the model correlation-polarization potential is used to include the correlation-polarization potential. The effect of nuclear dynamics on the collision probabilities is discussed comparing calculated total cross sections using the rovibrational close-coupling and the rotational LFCC method with other theoretical calculations and experimental results. The discussion includes comparison of the present vibrational $0 \rightarrow 1$ excitation process with the theoretical and measured values. The other vibrational and rotational elastic and excitation cross sections are also compared with the existing theoretical results and we have discussed the relevance of the effect of nuclear rotational and vibrational dynamics. We have also presented a comparison among the energy transfer parameters using different coupling schemes and have discussed the implications of the results.

DOI: 10.1103/PhysRevA.96.042709

I. INTRODUCTION

Understanding the nature of the interaction between the subatomic particles positron (electron) collision with an atom or molecule plays an important role in the field of research works [1–5]. To calculate the collision cross sections theoretically for such collision processes the interaction between the projectile and the electrons of the targets is included via the so-called static and polarization potential. In the case of a positron as a projectile the repulsive static potential and the attractive polarization potential cancel each other and give an effective potential. Thus for low-energy collision processes when a positron spends a longer time close to the targets, accurate calculations of these potentials are very important, especially the polarization potential. The necessity of accurate determination of the polarization potential is described by Tenfen *et al.* [6] who used this *ab initio* polarization potential for the positron-N_2 collision process in getting fairly good results comparing to recent measurement of collision cross sections. Although the calculation of *ab initio* potential has to be used to get more accurate theoretical results, the determination of this potential is a very complicated task for any system. Thus one has to rely on some approximate and reliable method to calculate this potential. One such model potential is positron correlation-polarization potential (PCOP) as proposed by Jain [7], especially designed for the positron as an incident particle. This model PCOP polarization potential has been applied successfully to the different positron collision processes and predicts reliable results except the appearance of minima structures in the theoretically calculated total cross sections. However, apart from the use of polarization potential, for multichannel calculation involving different quantum states of the target in the collision processes, the inclusion of the state-to-state coupling effect between the different states is also very important to get reliable results. This coupling effect for the positron-atom collision where atomic electronic states are involved is described in [8]. For molecular collision processes the situation is more complicated as apart from the molecular electronic states the rotational and vibrational states of the molecule are also included in the calculation in the multichannel formalism to account for the rotational and vibrational motions of the nuclei. The inclusion of these nuclear dynamics is necessary, especially in the lower-energy region where the incoming projectile spends a longer time with the target molecule and strongly interacts with it. Several theoretical works have been carried out for different systems with the positron as the projectile; viz., the works of Tenfen *et al.* [6], Mukherjee *et al.* [9], Gianturco and Mukherjee [10], Mukherjee and Sarkar [11], and Mukherjee and Mukherjee [12] using different coupling schemes, namely, rotational laboratory frame close coupling (rotational LFCC), body fixed vibrational close coupling (BFVCC), rovibrational close coupling (for details see [3,10,13–15]), and the method of continued fractions (MCF) and its multichannel version (MCF-MC) [16,17]. These methods are in accordance with how the nuclear motions are taken into account in the calculations.

All the calculations mentioned above [6,9–12,16,17] have been done for homonuclear diatomic molecules like H_2 and N_2 which have no permanent dipole moments. The heteronuclear molecule has a permanent dipole moment due to its asymmetric charge distribution. The body-frame

*tapas.mukherjee1@gmail.com

adiabatic nuclei approximation when applied to this kind of molecule produces infinite total cross sections. In the adiabatic nuclei approximation, where the rotational and vibrational motions of the molecule are treated adiabatically, the multiple extracted adiabatic nuclei (MEAN) approximation [18] has been employed to get convergent cross sections. On the other hand, the dynamically included nuclear motion (rotation and vibration) of the molecule in the calculation reduces the effect of the asymmetric charge distribution at large distance giving the finite effective potential which produces finite cross sections. Thus the close-coupling methods, which include the nuclear motions in dynamical equations of the collision process, are very suitable to get the finite cross sections for the molecules which have a permanent dipole moment like CO. Not only that, but also these methods give the rotational and vibrational state-to-state excitation cross sections which are important for understanding the nature of interaction and coupling effects as well as for the usefulness of the molecules in different areas. Earlier theoretical calculations have been done for CO using the rotational LFCC method by Ghosh *et al.* [19], the BFVCC method by Gianturco *et al.* [20], and the MCF method by Arretche *et al.* [21]. Recently elastic and inelastic vibrational cross sections for this molecule have been calculated by Tenfen *et al.* [22] employing the same MCF method as used by Arretche *et al.* [23], extending this MCF method to the multichannel case (MCF-MC) method. Among the different close-coupling methods the rovibrational close-coupling method is an elaborate and extensive way to include the rotational and vibrational motion of the nuclei in a dynamical way through the solution of coupled differential equations for the projectile. Here we have carried out the calculation for a positron collision with a CO molecule using rovibrational close-coupling methods where the PCOP potential is used as a polarization potential. The rotational and vibrational state-to-state coupling potentials [the matrix elements of total (static+correlation polarization) potential between different rotational and vibrational states] are evaluated to solve the coupled equations using rotational and vibrational wave functions corresponding to different rovibrational states. The motivation of the present study is to see the dynamical coupling effect of the rotational and vibrational state-to-state potentials on the scattering parameters for a CO molecule which has a finite dipole moment. Moreover, to estimate the effect of the vibrational motion only, here we have presented the results using a decoupled form of rotational and vibrational motion, viz., the laboratory frame rotational close coupling with adiabatic nuclear vibration (LFCC-ANV) scheme where rotational motions are included through close-coupling calculation, but the vibrational motions are taken into account in an adiabatic way.

We present here the total angle-integrated cross sections (summed over rotation and vibration cross sections), vibrational angle-integrated elastic and state-to-state excitation cross sections (summed over rotational cross sections), and rotational angle-integrated elastic state-to-state cross sections up to 7.0 eV (which is below the positronium formation threshold). Here we have also recalculated the total and rotational cross sections using the rotational LFCC method. This calculation was previously done by Ghosh *et al.* [19] and the reasons behind this recalculation are described in the Results and Discussions section. The present results are compared with some of the existing theoretically calculated results. The results are also compared with the experimentally measured values by Sullivan *et al.* [4], Kwan *et al.* [23], Sueoka and Hamada [24], and Zecca *et al.* [25].

A. Theory

The detailed theoretical calculations for the rovibrational close-coupling methods are presented in our earlier calculations [11,12]. Here we have also presented the same which have been used to compute the collision parameters. The theoretical collision parameters are obtained solving the following Schrödinger equation for the total positron-molecule system:

$$(H - E)\Psi = 0, \tag{1}$$

with the usual scattering boundary conditions for collision calculation.

Here H and Ψ are the total Hamiltonian and the total wave function of the positron-molecule system. In the present case of a positron–carbon monoxide molecule collision process under the (electronically elastic) rovibrational close-coupling method under Born-Oppenheimer approximation the total Hamiltonian H of the system is given by

$$H \equiv H(\vec{r}_p) + H_{\rm el}(\vec{r}_e) + H_{\rm vib}(R) + H_{\rm rot}(\widehat{R}) + V_{p-{\rm mol}}(\vec{r}_p,\vec{r}_e,\vec{R}), \tag{2}$$

where $\vec{r}_p$ is the positron coordinate measured from the center of mass of the system, $\vec{r}_e$ collectively denotes the molecular electronic coordinates, and $\vec{R}$ is the internuclear set of coordinates of the molecule. $H(\vec{r}_p)$ is the kinetic energy operator for the incident positron; $H_{\rm vib}(R)$, $H_{\rm rot}(\widehat{R})$, and $H_{\rm el}(\vec{r}_e)$ are the vibrational, rotational, and electronic Hamiltonians of the target molecule, respectively. $V_{p-{\rm mol}}(\vec{r}_p,\vec{r}_e,\vec{R})$ represents the positron-molecule interaction. The total wave function Ψ is characterized by, for the present method, the electronic, vibrational, and rotational quantum numbers of the molecule and the angular momentum quantum number of the projectile particle $0,v,j,l$, respectively, and is described by

$$\Psi^{JM}_{0vjl}(\vec{r}_p,\vec{r}_e,\vec{R}) = \chi_0(\vec{r}_e,\vec{R}) \sum_{\alpha''} r_p^{-1} u^{Jvjl}_{v'j'l'}(r_p) \mathbf{Y}^{JM}_{j'l'} \times (\widehat{r}_p,\widehat{R})\phi_{v'}(R), \tag{3}$$

where $\chi_0(\vec{r}_e,\vec{R})$ is the ground-state electronic wave function which parametrically depends on $\vec{R}$. $\phi_{v'}(R)$ is the vibrational wave function of the molecule. The angular basis function $\mathbf{Y}$ is given by

$$\mathbf{Y}^{JM}_{j'l'}(\widehat{r}_p,\widehat{R}) = \sum_{m_j}\sum_{m_l} \langle jlm_jm_l \mid jlJM\rangle \mathbf{Y}_{lm_l}(\widehat{r}_p)\mathbf{Y}_{jm_j}(\widehat{R}). \tag{4}$$

The coefficients $\langle jlm_jm_l \mid jlJM\rangle$ are the familiar Clebsch-Gordan coefficients. $\mathbf{Y}_{jm_j}(\widehat{R})$ and $\mathbf{Y}_{lm_l}(\widehat{r}_p)$ are the nuclear rotational and positron angular wave functions, respectively. In the present formalism $\vec{J} = \vec{j} + \vec{l}$ and its projection M along

the nuclear axis are the good quantum numbers (constant of motion) of the system.

Using the above Hamiltonian and wave function in the Schrödinger equation (1) one gets the corresponding rovibrational close-coupled differential equation,

$$\left[\frac{d^2}{dr_{r_p}^2} - \frac{l'(l'+1)}{r_p^2} + k_{\alpha\alpha'}^2\right] u_{\alpha'}^{Jjl}(r_p) = \sum_{\alpha''} \langle \alpha', J|V'(\vec{r}_p,\vec{R})|\alpha'', J\rangle u_{\alpha''}^{Jjl}(r_p), \quad (5)$$

where α collectively denotes the quantum numbers v, j, l.

$$V'(\vec{r}_p,\vec{R}) = \int \chi_0(\vec{r}_e,\vec{R}) V_{p-\mathrm{mol}}(\vec{r}_p,\vec{r}_e,\vec{R}) \chi_0(\vec{r}_e,\vec{R}) d\vec{r}_e, \quad (6)$$

$$k_{jj'vv'}^2 = 2(E - \varepsilon_{jj'} - \varepsilon_{vv'}), \quad (7)$$

where E is the incident positron energy. $\varepsilon_{jj'}$ and $\varepsilon_{vv'}$ are the energy differences between rotational levels j and j' and the vibrational levels v and v', respectively.

The rotational and vibrational state-to-state coupling potential matrix elements used in the coupled equations are given by the following relation:

$$\langle v'j'l'|V'(\vec{r}_p,\vec{R})|v''j''l''\rangle = 2\iiint \phi_{v'}(R)\mathbf{Y}_{j'l'}^{JM*}(\hat{r}_p,\hat{R})V'(\vec{r}_p,\vec{R})\phi_{v''}(R)Y_{j''l''}^{JM} \times (\hat{r}_p,\hat{R}) dR d\hat{R} d\hat{r}_p. \quad (8)$$

Here the interaction potential has been expanded in terms of Legendre polynomials as

$$V'(\vec{r}_p,\vec{R}) = \sum_\lambda v_\lambda(r_p,R) P_\lambda(\hat{r}_p,\hat{R}). \quad (9)$$

Equation (8) takes the final form as (after angular integration over the nuclear and positron angular coordinates $\hat{R}$ and $\hat{r}_p$ respectively)

$$\langle v'j'l'|V'(\vec{r}_p,\vec{R})|v''j''l''\rangle = \sum_\lambda \langle v'(R)|v_\lambda(r_p,R)|v''(R)\rangle f_\lambda(j',l',j'',l'';J). \quad (10)$$

$f_\lambda(j',l',j'',l'';J)$ is the angular coupling factor given by (Lane and Geltman [14])

$$f_\lambda(j',l',j'',l'';J) = (-1)^{j'+j''-J}(2\lambda+1)^{-1} \times [(2j'+1)((2l'+1)(2j''+1)(2l''+1)]^{1/2} \times (l'l''00|l'l''\lambda 0)(j'j''00|j'j''\lambda 0) W(j'l'j''l'';J\lambda). \quad (11)$$

$(ab00|ab\lambda 0)$ and $W(j'l'j''l'';J\lambda)$ are the familiar Clebsch-Gordan and Racah coefficients, respectively.

In Eq. (10) the integration is over the nuclear coordinate R only.

To calculate the potential matrix elements the vibrational wave functions of the molecule are calculated using the following differential equations:

$$\left\{\frac{d^2}{dR^2} + 2\mu[\varepsilon_v - \varepsilon(R)]\right\}\phi_v(R) = 0, \quad (12)$$

where μ is the reduced mass of the molecule and $\varepsilon(R)$ is electronic energies for different nuclear geometries which support the different vibrational bound states.

The static potential is calculated using a ground-state wave function of the molecule. To calculate the polarization potential which takes into account the effect of distortion of the molecule in the presence of a positron as well as the effect of correlation, the well known model positron correlation-polarization potential (PCOP), specially designed to describe the interaction between the positron and distorted molecule, is used. Detailed discussions and its functional form are given elsewhere, viz., in [11].

The solution of rotationally and vibrationally coupled differential equations give the T-matrix elements $T^J(v'j'l',vjl)$ and using these elements we have calculated rotationally elastic and state-to-state ICS (angle-integrated cross section), vibrationally elastic and state-to-state ICS (summed over rotational ICS), and the total cross section TCS (summed over rotational and vibrational ICS). We have also calculated rotationally elastic and state-to-state ICS and TCS (summed over rotational ICS) using the rotational LFCC method. To get LFCC-ANV vibrational state-to-state cross sections first we calculate total cross sections solving the rotational LFCC differential equation [13,14] for different internuclear separation and these cross sections are then integrated between different vibrational states which give the LFCC-ANV vibrational state-to-state cross sections.

Here we have also calculated the average vibrational (rotational) energy transfer, defined as

$$\langle \Delta E_\alpha \rangle = \frac{\sum_{\alpha\neq 0}^{\alpha'} \Delta E_{\alpha\to\alpha'}\sigma(\alpha\to\alpha')}{\sum_{\alpha=0}^{\alpha'}\sigma(\alpha\to\alpha')}, \quad (13)$$

where $\sigma(\alpha\to\alpha')$ is the state-to-state cross section, $\Delta E_{\alpha\to\alpha'}$ is the energy difference between the vibrational (rotational) states, and α denotes the vibrational (rotational) quantum number corresponding to different states of the molecule. This term describes the overall probability of transferring energy into the molecular degrees of freedom from a given initial level (here vibrational and rotational levels are defined by $v = 0$ and $j = 0$). This energy transfer index also indicates the relative efficiency of rotationally and vibrationally inelastic collision. The higher value of this index indicates higher efficiency of cooling of a hot positron in a molecular gas environment.

B. Computational details

To calculate the static and polarization potentials we have used Slater-type (STO) self consistent field (SCF) ground-state electronic wave functions at various internuclear separation R ranging from $1.8a_0$ to $2.483a_0$ according to McLean and Yoshimine [26]. The vibrational coupling potentials are calculated using the vibrational wave function $\phi_v(R)$. These wave functions are obtained by solving Eq. (4) using potential energy values calculated by Peng-Fei *et al.* [27]. The coupled differential equation [Eq. (2)] is solved using the variable

TABLE I. Vibrational and rotational threshold energies (in meV) for CO molecule. v and j label the vibrational and rotational quantum numbers, respectively.

	$v=0$			1				2				3				4			
$j=0$	1	2	3	0	1	2	3	0	1	2	3	0	1	2	3	0	1	2	3
0.0	0.47	1.4	3.0	265	266	267	286	527	528	529	531	786	787	788	789	1042	1043	1044	1045

step-size Numerov method up to the radial distance of positron $100a_0$ measured from the center of mass of the molecule and obtained the T-matrices and hence the required cross sections. To get the converged cross sections the static potential is calculated up to the angular momentum $\lambda_{\max} = 13$. It is to be noted here that due to the heteronuclear nature of the CO molecule, all even and odd momenta are included in the calculation. The equations are solved for a maximum of five vibrational states ($v = 0 \rightarrow 4$) and five ($j = 0 \rightarrow 4$) rotational states. The maximum number of partial waves $l_{\max} = 7$ and maximum total quantum number $J_{\max} = 7$ ($J = j + l$) are the other parameters to specify the angular motions of the positron and the molecule. In this calculation we have only included open channels whose numbers as well as the number of coupled channels depend on the energy of the incident positron and the energy of the corresponding vibrational and rotational states. The maximum number of coupled equations solved is 45. In Table I we have tabulated the rotational and vibrational threshold energies for a CO molecule.

II. RESULTS AND DISCUSSIONS

A. Coupling potentials

In the close-coupling method two types of coupling appear; one is potential coupling and the other is dynamical coupling.

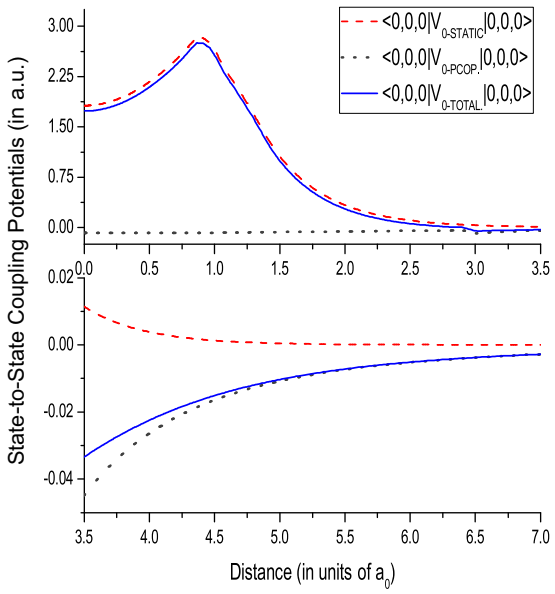

FIG. 1. Present computed rovibrational state-to-state coupling potentials for spherical ($\lambda = 0$) components for vibrationally elastic and rotationally elastic cases. The potential matrix elements are defined in the text.

The potential coupling is represented by the state-to-state coupling potential matrices and is represented by the terms $\langle v,j,l|v_\lambda|v',j',l'\rangle$ in the close-coupled differential equation (5). The dynamical coupling represents the influence of different channels (state-to-state coupling effects) on the result of a particular channel during the collision process. This dynamical coupling effect is included in the close-coupling method when one solves the coupled differential equation (5). To get the essence of the nature of the coupling forces during the collision process, which is responsible for transition between different states, we start our discussions on the state-to-state potential coupling. Before discussing the behavior of such coupling potentials we first present the comparison between the static and correlation-polarization potential used in the calculation. In Fig. 1 we have plotted spherical components of those potentials with the total (static+correlation polarization) potentials for the elastic channel case. The figure shows that near the vicinity of the molecule the static potential strongly dominates over the PCOP potential. Above the distance $3.5a_0$ from the center of mass of the molecule the PCOP potential is stronger than the static potential, although the strength of the potentials are less in comparison to the static potential near the center of mass of the molecule.

A number of coupling potentials appear in solving Eq. (5) whose number depends on the number of vibrational (v), rotational (j) states of the molecule as well as the number of partial waves l that are included in the calculation. Some of such state-to-state potentials are plotted below (Figs. 2–6). In Fig. 2 we have plotted vibrationally elastic and rotationally elastic, $\langle 0,0,0|v_{0\text{-tot}}|0,0,0\rangle$, and vibrationally elastic but rotationally inelastic, $\langle 0,1,1|v_{1\text{-tot}}|0,0,0\rangle$, $\langle 0,2,2|v_{2\text{-tot}}|0,0,0\rangle$, coupling potentials for three different moments (spherical and nonspherical components: $\lambda = 0,1,2$). Here the symbol "-tot" represents calculated total (static+correlation polarization) potential using the electronic wave function of the molecule. The graphs show that the differences among the strengths of the potentials for a vibrationally elastic channel are comparable to each other. But an interesting feature is evident from the figure that the variation of the potential with the distance for $\lambda = 1$ is opposite to those for $\lambda = 0,2$ (signs of the potentials are opposite) which implies that cancellation occurs among the different potentials (depending on λ) when one solves the coupled differential equations. This special feature is the nature of a heteronuclear molecule like CO, which is not observed in the case of a homonuclear molecule like H_2 or N_2 (see [12]). This feature is based on the behavior of the molecules belonging to different molecular symmetries. It will be clear from the following discussions on the calculation point of view. The potentials $v_\lambda(r_p, R)$, defined in Eq. (9), are calculated using the charge density of the molecule which is expanded in terms of Legendre polynomials $P_\lambda(\hat{r})$ as $\rho(\vec{r}) = \sum_\lambda a_\lambda(r) P_\lambda(\hat{r})$. The

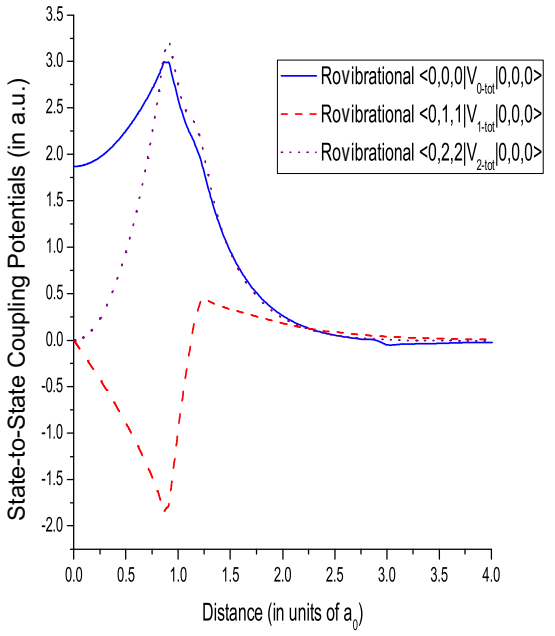

FIG. 2. Present computed rovibrational state-to-state coupling potentials for spherical and nonspherical ($\lambda = 0,1,2$) components for vibrationally elastic and rotationally both elastic and inelastic cases. The potential matrix elements are defined in the text.

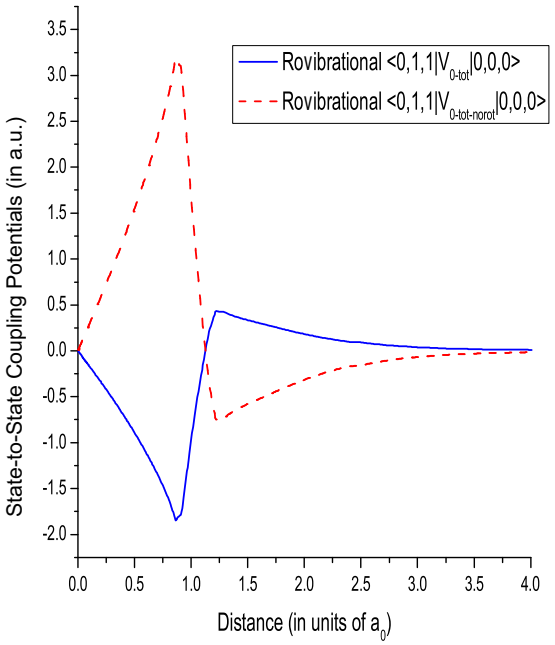

FIG. 3. Present computed rovibrational state-to-state coupling potentials for spherical ($\lambda = 0$) components. The potential matrix elements are defined in the text.

sign of $a_\lambda(r)$ depends on even and odd values of λ. The sign for even λ is opposite to that for odd λ. As the CO molecule belongs to the point group $C_{\infty v}$ all λ coefficients $a_\lambda(r_p,R)$ are nonzero whereas, because of the inversion symmetry that characterizes the molecules like H_2 and N_2 belonging to the point group $D_{\infty h}$, only the even-λ coefficients $a_\lambda(r_p,R)$ are nonzero. The magnitude and sign of the state-to-state coupling potentials depend on $v_\lambda(r_p,R)$ and hence the values of coefficients $a_\lambda(r_p,R)$ and λ.Thus the sign of the potentials for H_2, N_2 are the same due to only the coefficients $a_\lambda(r_p,R)$ for even values of λ being nonzero whereas for the CO molecule the potentials' values are both positive and negative due to all λ coefficients $a_\lambda(r_p,R)$ being nonzero which is also evident from Fig. 2.

In Fig. 3 we have compared the calculated values between the spherical components ($\lambda = 0$) for a vibrationally elastic and rotationally inelastic channel $V_{0\text{-tot}}$ potential. Here we have also plotted the $V_{0\text{-tot-norot}}$ potential, where "norot" implies that the angular coupling factor $f_\lambda(j',l',j'',l'';J)$ by which the rotational state-to-state coupling effect is included [defined in Eq. (11)] through the solution of the coupled differential equations is not multiplied with this component. This last component is shown here for comparison only but not used in the present calculation. It is evident from the figure that the two potentials not only vary oppositely but the strength of the potential also differs. This shows the importance of the inclusion of the effect of rotational motion in the calculation of the rovibrational coupling potential.

To estimate the effect of the vibrationally elastic channel the spherical components of the vibrational coupling potential $\langle 0,0,0|v_{0\text{-tot}}|0,0,0\rangle$ and rotational $\langle 0,0|v_{0\text{-tot}}|0,0\rangle$ coupling potential (the last one is defined by $\langle j,l|v_\lambda|j',l'\rangle$) are plotted in Fig. 4. The figure shows that the values marginally differ with each other. This feature is also seen for nonspherical components ($\lambda = 0,2$) also (not shown here). Thus it is evident that the vibrational ground state has less significant effect on the total coupling potential.

To compare the strength of the different vibrationally "elastic" potentials we have plotted the spherical components of the coupling potential, $\langle 0,0,0|v_{0\text{-tot}}|0,0,0\rangle$, $\langle 1,0,0|v_{0\text{-tot}}|1,0,0\rangle$, and $\langle 2,0,0|v_{0\text{-tot}}|2,0,0\rangle$, in Fig. 5. Note that the last two components are elastic in the sense that the vibrationally initial and final channels for the respective components are

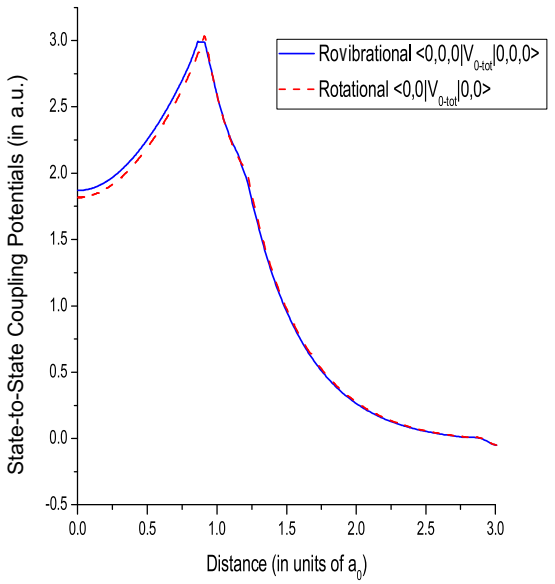

FIG. 4. Present computed rovibrational and rotational state-to-state coupling potentials for spherical ($\lambda = 0$) components. The potential matrix elements are defined in the text.

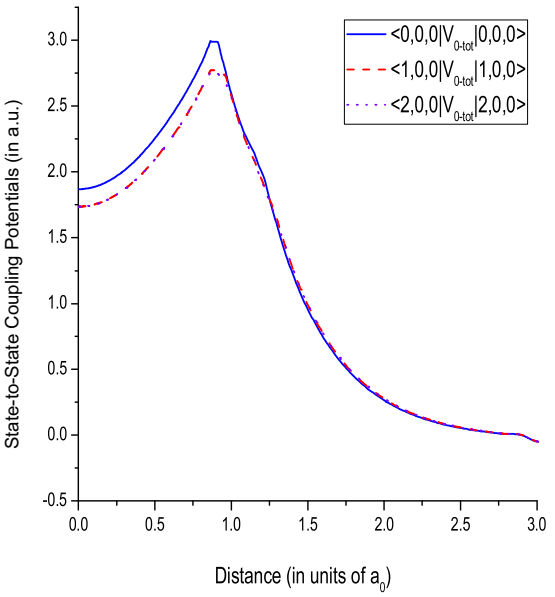

FIG. 5. Present computed rovibrational state-to-state coupling potentials for spherical ($\lambda = 0$) components. The potential matrix elements are defined in the text.

the same although they correspond to the vibrationally excited states. The figure shows that the nature of the variation of the potentials with the distance is the same, and the strengths of the potentials are also almost the same, $\langle 0,0,0|v_{0\text{-tot}}|0,0,0\rangle$; the component involving the vibrational ground state for both initial and final channels is slightly higher.

In Fig. 6 we have plotted the potentials for vibrationally inelastic channels $\langle 1,0,0|v_{0\text{-tot}}|0,0,0\rangle$ and $\langle 2,0,0|v_{0\text{-tot}}|0,0,0\rangle$ (the initial vibrational states are different). It is evident from the figure that unlike the elastic potentials shown in Fig. 4

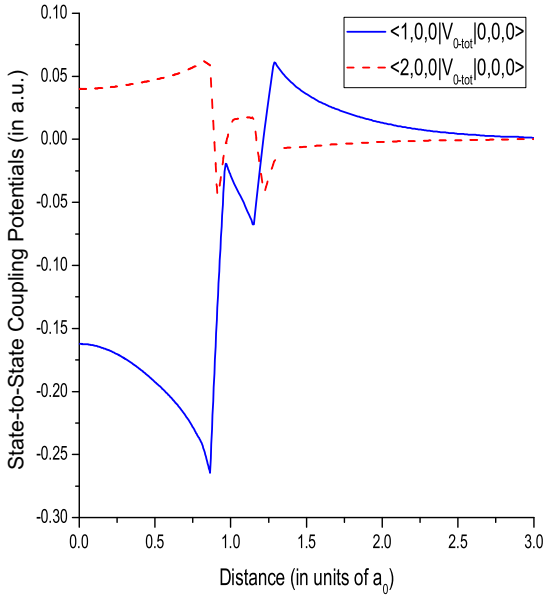

FIG. 6. Present computed rovibrational state-to-state coupling potentials for spherical ($\lambda = 0$) components. The potential matrix elements are defined in the text.

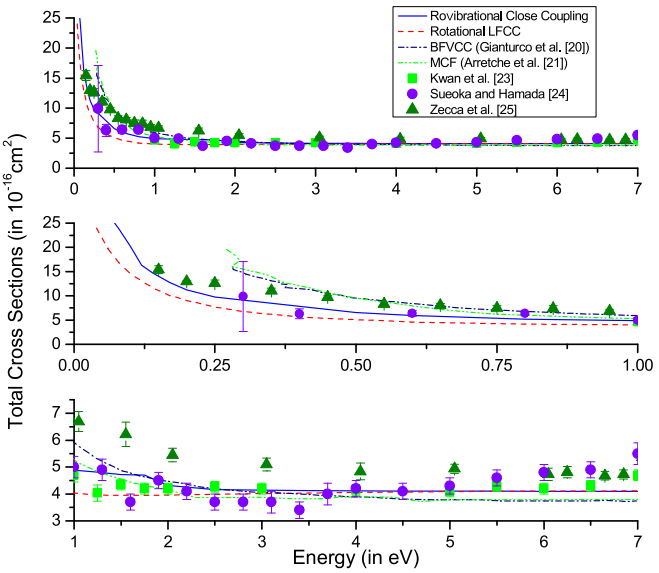

FIG. 7. Upper panel: Present computed angle-integrated rovibrational and rotational LFCC total cross sections along with the BFVCC result of Gianturco *et al.* [20] and Arretche *et al.* [21], for the positron–carbon monoxide molecule collision process. Different measured values by Kwan *et al.* [23], Sueoka and Hamada [24], and Zecca *et al.* [25] are also plotted for comparison. Middle panel: Same as upper panel but in the lower-energy region. Lower panel: Same as upper panel but in the higher-energy region.

the nature and strength of these two inelastic potentials differ from each other. However, the strength of the potentials is less compared to the elastic components.

B. Total and vibrational elastic cross section

In Fig. 7 we present the computed angle-integrated total (summed over rotational and vibrational) cross sections using both rovibrational and rotational LFCC close-coupling methods, the BFVCC results of Gianturco *et al.* [20], and the MCF results of Arretche *et al.* [21] which are plotted up to 7.0 eV (below positronium formation threshold). The measured values of Kwan *et al.* [23], Sueoka and Hamada [24], and Zecca *et al.* [25] are also plotted for comparison. As the top panel shows the cross sections that are hard to distinguish we separately plot two more curves in the same figure. In the middle panel we plot the cross sections for lower energy (up to 1.0 eV) and in the lower panel we plot the results for higher energy (ranging from 1.0 to 7.0 eV). It is to be mentioned here that earlier the same collision process was investigated by Ghosh *et al.* [19] employing the rotational LFCC method. In that calculation they used the near–Hartree-Fock (HF) ground-state electronic wave function of the CO molecule in terms of a Gaussian-type orbital (GTO) basis set as used by Jain [28] to calculate the static and correlation-polarization (PCOP) potentials. Moreover, that calculation only includes the dipole moment of the molecule. In the present calculation the Slater-type orbital (STO) basis set and all the multipole moments (for different λ ranging from $\lambda = 1$ to $\lambda_{\max} = 13$) have been employed. The main motivation of the present calculation is to see the effectiveness

of inclusion of the dynamical coupling effect of different molecular degrees of freedom (rotational and vibrational) using different coupling schemes in determination of collision parameters. Thus here we have recalculated the cross sections using the rotational LFCC method with the same STO basis set to describe the electronic ground state and the moments which also have been used to calculate the cross sections using the rovibrational close-coupling method. However, we have found some differences between the present results and the results of Ghosh *et al.* in the lower-energy region. Theoretically, Gianturco *et al.* performed the calculation using the body-fixed vibrational close-coupling (BFVCC) method with the same STO basis set as used in the present calculation. However, the potential energy values used to calculate the vibrational wave function are different from the present one. Arretche *et al.* used the fixed nuclei framework and employed the method of continued fractions (MCF). The near–Hartree-Fock wave function using the Gaussian basis set at the equilibrium geometry was used in their calculation. It is to be mentioned that Tenfen *et al.* [22] also carried out the calculation for the same collision process using the BFVCC scheme. They compared the calculated ICS 00 [integral cross section for vibrationally elastic case ($v = 0 \rightarrow v' = 0$)] with experimental TCS (total cross sections) considering the very low values of vibrational excitation cross sections in comparison to the elastic results and these calculated values are very similar to the MCF results of Arretche *et al.* Thus here we have plotted the results of Arretche *et al.* in the figure. It is seen from the figure that in the lower-energy region there are differences among the different theoretical results (however, the BFVCC and MCF results match each other). In the higher-energy region all theoretically calculated results almost merge with each other. From the figure it is also important to notice that the present rovibrational and the rotational LFCC results do not match each other in the lower-energy region; the rovibrational close-coupling result is higher. In Fig. 4 we have seen that the strength and variation of the state-to-state coupling potential for elastic channels are almost the same, calculated using the rotational LFCC and rovibrational methods. Thus the difference of the results is due to the effect of the vibrationally inelastic state-to-state coupling potential which is absent in the rotational LFCC formalism. However, for the rovibrational method the effect of rotational coupling remains effective by the angular coupling factor $f_\lambda(j',l',j'',l'';J)$ in the coupling potential. Higher values of rovibrational cross sections imply the more attractive nature of vibrational coupling in comparison to the rotational coupling. This is also evident if we compare our present results with the BFVCC result. It is seen that the BFVCC values are higher than the present results. In the BFVCC scheme rotational motion of the molecule is not included in the calculation and the resulting cross section is only the effect of vibrational motion, which produces higher values of cross section. But in the present rovibrational formalism the combined rotational and vibrational effect is not strong enough to get values comparable to the BFVCC result. This feature for the positron–carbon monoxide collision process is different from that of a positron–nitrogen molecule collision. In the case of the nitrogen molecule the rotational LFCC result is lower than the rovibrational result [12] similar to the present case whereas the rovibrational cross section is higher than

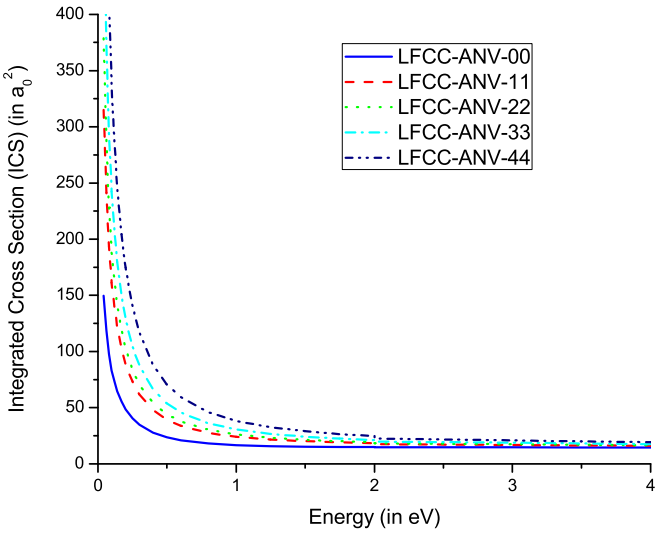

FIG. 8. Present computed angle-integrated vibrational elastic cross sections using LFCC-ANV (see the text) method for the positron–carbon monoxide molecule collision process.

the BFVCC result, opposite to that of positron collision with a carbon monoxide molecule. It seems the rotational effect for the case of a carbon monoxide molecule is stronger than for the case of a nitrogen molecule. Another interesting case is evident from the figure, that unlike the case of the hydrogen and nitrogen molecules here no minimum appears in the calculated integrated cross sections, which is supposed to be due to the lack of inclusion of the polarization effect in the model PCOP potential which is used here. In this connection we refer to the work of Tenfen *et al.* [22] where they have found the minimum structure appears in all calculated vibrationally elastic cross sections (VECS) using the MCF-MC method. While searching for the cause behind this they have concluded that the multichannel coupling effect is responsible for the generation of minimum structure. To show this they have calculated vibrationally elastic cross sections (VECS) using diagonal components of a vibrational potential matrix and data show the expected increase of the VECS with the vibrational quantum numbers. Here we have also calculated the VECS using the LFCC-ANV method where the rotational states are coupled but the vibrational states are included adiabatically. The computed results are presented in Fig. 8 where we see that the nature of variation of the VECS with vibrational quantum number agrees with the VECS of Tenfen *et al.* [22] calculated with the diagonal vibrational potential. However, it is interesting to see that in the present LFCC-ANV results no such minimum appears in the VECS although the multichannel effect is still present due to rotational coupling included in the rotational LFCC method. Thus the disappearance of the minimum in the total cross section computed using all the theoretical methods (Fig. 7) as well as in the present calculated vibrational elastic cross section (VECS) employing the LFCC-ANV method, and on the other hand the appearance of the minimum in VECS calculated using the MCF-MC method, shows the importance of the rotational coupling effect in the positron–carbon monoxide collision process. It seems that the vibrational multichannel coupling effect which

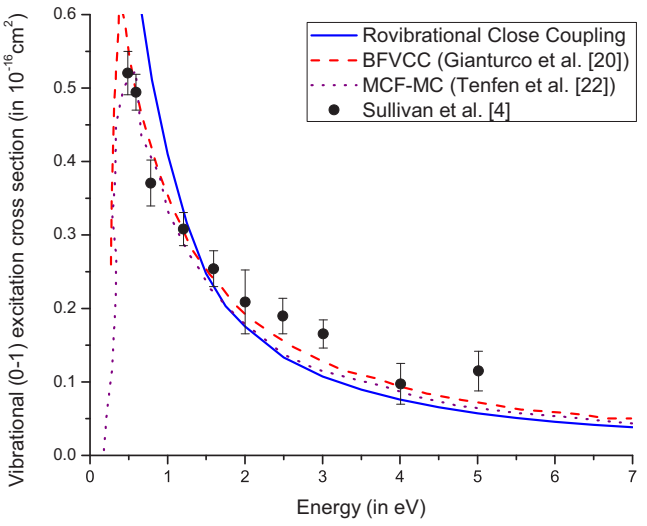

FIG. 9. Comparison between present computed angle-integrated vibrational state-to-state $0(v) \rightarrow 1(v')$ excitation cross sections with other theoretical results and measured values for positron–carbon monoxide molecule collision.

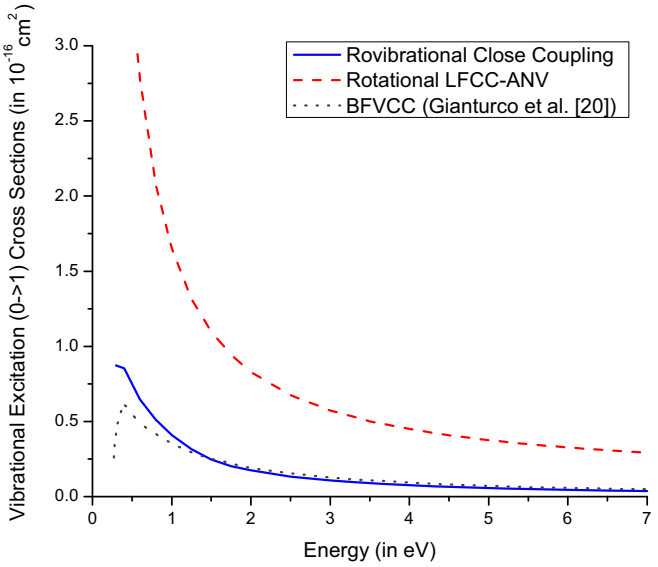

FIG. 10. Comparison between present computed angle-integrated vibrational state-to-state $0(v) \rightarrow 1(v')$ excitation cross sections using rovibrational and LFCC-ANV methods and BFVCC result for positron–carbon monoxide molecule collision.

generates the minimum in VECS as described by Tenfen *et al.* [22] is reduced by the rotational coupling effect. Comparison of the calculated values with the measured data shows that the present rovibrational TCS well match with the experimental results of Kwan *et al.* and the results of Sueoka and Hamada in the whole energy range presented here, while they well agree with Zecca *et al.* in very low and higher energy values. On the other hand the BFVCC and MCF results better agree with the measured values of Zecca *et al.* It is seen from the figure that there are differences between the experimental data measured by different authors. The reason behind the different values of the measurements is not clear and needs more theoretical and experimental studies. However, Zecca *et al.* attributed the difference of their experimental values from the other experimental values to the superior angular resolution of their apparatus to those of other apparatuses.

C. Vibrational and rotational inelastic cross section

In Fig. 9 the present rovibrational angle-integrated excitation cross sections (vibrational inelastic ICS) for vibrational $0 \rightarrow 1$ (summed over rotational states) transition process is plotted which is calculated using the rovibrational coupling scheme along with the theoretical BFVCC result of Ginnturco *et al.* [20] and the MCF-MC result of Tenfen *et al.* [22]. The experimental result of Sullivan *et al.* [4] is also included for comparison. It is seen from the figure that the present results well agree with the measured values and other theoretical results with some marginal differences. However, an interesting difference between the present result and the theoretical results is seen around the threshold of vibrational excitation. The present calculated cross section varies smoothly whereas the other calculations generate a peak around the threshold. In this juncture we want to make some comments on the excitation threshold of the vibrational $0 \rightarrow 1$ transition. This threshold value is 0.266 eV as mentioned by Gianturco *et al.* [20] and Tenfen *et al.* [22]. However, for the present rovibrational formalism one cannot specify a particular value of vibrational excitation threshold as the excitation involves different rotational levels of the excited vibrational states. Thus (shown in Table I) the vibrational excitation threshold varies from 0.265 to 0.286 eV depending on the transition from ground vibrational and rotational level to the rotational quantum number j of the excited vibrational state. However, if we define the vibrational excitation threshold as the energy required for transition from ground vibrational state to ground rotational state of the excited vibrational states, then the excitation threshold for the vibrational $0 \rightarrow 1$ transition is 0.265 eV, which is almost same as the above-mentioned results of Gianturco *et al.* and Tenfen *et al.* [22].

The present calculation includes both rotational and vibrational dynamics whereas both BFVCC and MCF-MC calculations include only the vibrational dynamics. Thus it seems that the disappearance of the peak in the present result is due to the effect of rotational dynamics. For more clear understanding of this we have also calculated the vibrational $0 \rightarrow 1$ cross section using the LFCC-ANV method and plotted it in Fig. 10 along with the rovibrational and BFVCC results. The figure shows that although the LFCC-ANV result is higher than the rovibrational result the nature of the variation of the both results is similar. Moreover, no peak in the cross section appears similar to the rovibrational result. This means that the rotational coupling effect is responsible for the disappearance of the peak in the rovibrational cross section.

In Figs. 11 and 12 we have plotted the present calculated ($0 \rightarrow 2$ and $0 \rightarrow 3$) vibrational excitation cross sections along with the results calculated using the BFVCC and MCF-MC methods, respectively. Both figures show that the cross sections for these excitation processes are less in magnitude compared to the $0 \rightarrow 1$ excitation process. Both cross sections show that the rovibrational results are higher than the BFVCC results in the lower-energy region and merge with each other with energy

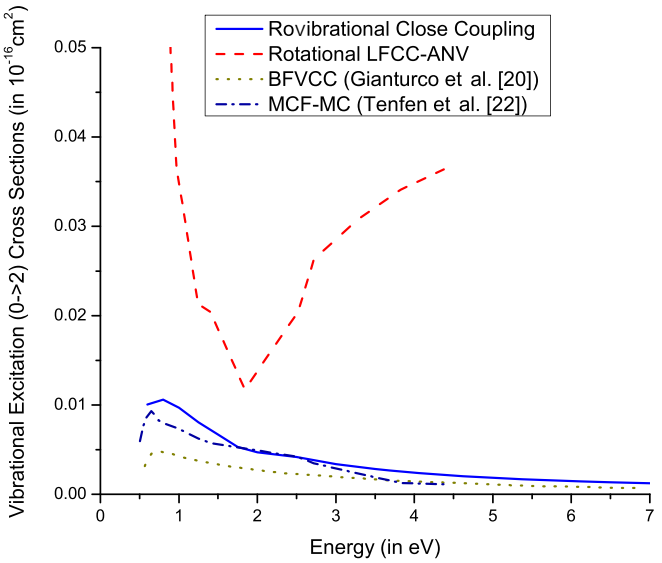

FIG. 11. Comparison between present computed angle-integrated vibrational state-to-state $0(v) \rightarrow 2(v')$ excitation cross sections using rovibrational and LFCC-ANV methods along with BFVCC and MCF-MC results for positron–carbon monoxide molecule collision.

which is the same as the $0 \rightarrow 1$ cross sections. On the other hand the $0 \rightarrow 2$ rovibrational results are higher and $0 \rightarrow 3$ values are lower than MCF-MC results in the lower-energy region. We have also presented LFCC-ANV results where $0 \rightarrow 2$ and $0 \rightarrow 3$ cross sections are high compared to the other theoretical values. The $0 \rightarrow 2$ results show a minimum whereas $0 \rightarrow 3$ results vary smoothly. The rotational LFCC-ANV data show that this method overestimates $0 \rightarrow 2$ and $0 \rightarrow 3$ cross sections. However, the values are very small and it is not possible to make any final comments on the variations and differences of the cross sections without comparing with the measured values.

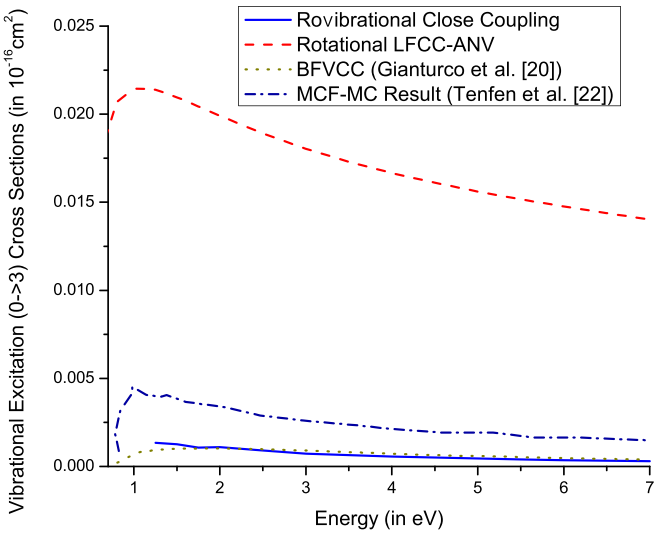

FIG. 12. Same as Fig. 11 but for $0(v) \rightarrow 3(v')$ vibrational excitation cross section.

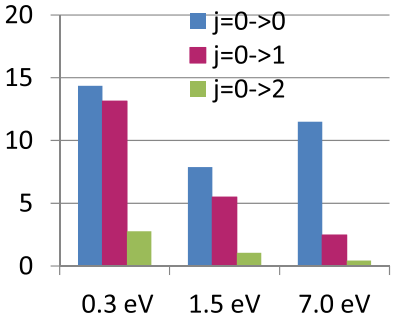

FIG. 13. Present computed angle-integrated rotational state-to-state elastic $0(j) \rightarrow 0(j')$, and excitation $0(j) \rightarrow 1(j')$ and $0(j) \rightarrow 2(j')$ cross sections for vibrational elastic $0(v) \rightarrow 0(v')$ process (in a_0^2) for positron–carbon monoxide molecule collision.

In the present work we have also calculated angle-integrated rotational cross sections for both elastic and excitation processes. It is to be mentioned that in the case of the rovibrational coupling scheme for each vibrational process (elastic and inelastic) there corrrespond several rotational elastic and inelastic processes. In Fig. 13 we have compared the rotational elastic $0 \rightarrow 0$ and inelastic $0 \rightarrow 1$ and $0 \rightarrow 2$ cross sections in the case of the vibrationally elastic (vibrational $0 \rightarrow 0$) channel for three different energies (these energies are chosen to cover the whole energy range considered here). It is seen from the figure that for all energies shown here the elastic $0 \rightarrow 0$ values are higher than the $0 \rightarrow 1$ and $0 \rightarrow 2$ values. However, for positron energies 0.3 and 1.5 eV $0 \rightarrow 1$ values are comparable to $0 \rightarrow 0$ values, whereas for 7.0 eV the $0 \rightarrow 0$ value is much higher. An interesting result is seen from the figure that for positron energy 7.0 eV the $0 \rightarrow 0$ cross section is higher than for 0.3 and 1.5 eV. This means that there are minima in the rotational $0 \rightarrow 0$ cross section. However, the total cross section for the vibrational $0 \rightarrow 0$ process is the sum of the rotational cross sections and this total value as well as the total cross section (which is the sum of the vibrational cross

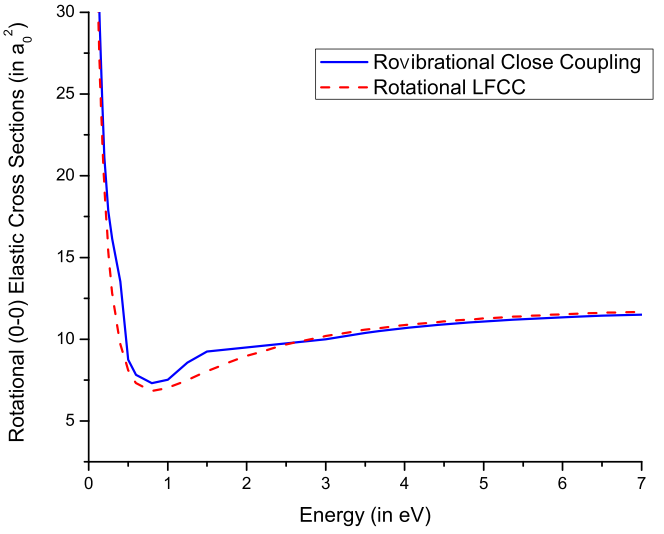

FIG. 14. Present computed angle-integrated rotational $0 \rightarrow 0$ (elastic) cross sections for the vibrational elastic process in positron–carbon monoxide molecule collision.

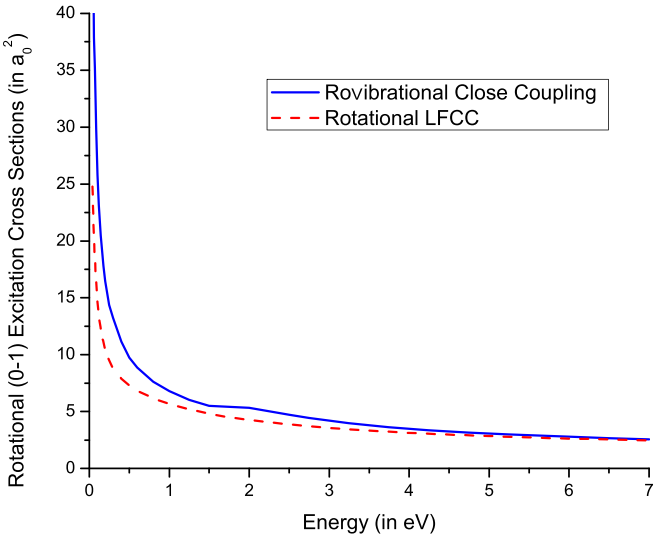

FIG. 15. Present computed angle-integrated rotational state-to-state $0 \rightarrow 1$ excitation cross section for vibrational elastic process in positron–carbon monoxide molecule collision.

sections) shows no minimum. To find the effect of vibrational motions we have compared the rotational elastic $0 \rightarrow 0$ and inelastic $0 \rightarrow 1$ and $0 \rightarrow 2$ cross sections for vibrationally elastic processes using the rovibrational coupling scheme with the results calculated employing the rotational LFCC method in Figs. 14–16. The figures show that the values and energy dependence using both methods are almost the same with a small difference in the case of rotational $0 \rightarrow 1$ cross sections in the low-energy region. This implies that the vibrational coupling effect has less influence on rotational cross sections in the vibrational elastic channel. Thus we see that in the present positron-CO collision process using close-coupling formalism the higher rotational excited state has a pronounced effect in determining the total collision cross section compared to the vibrational effect when the molecule is in its ground vibrational

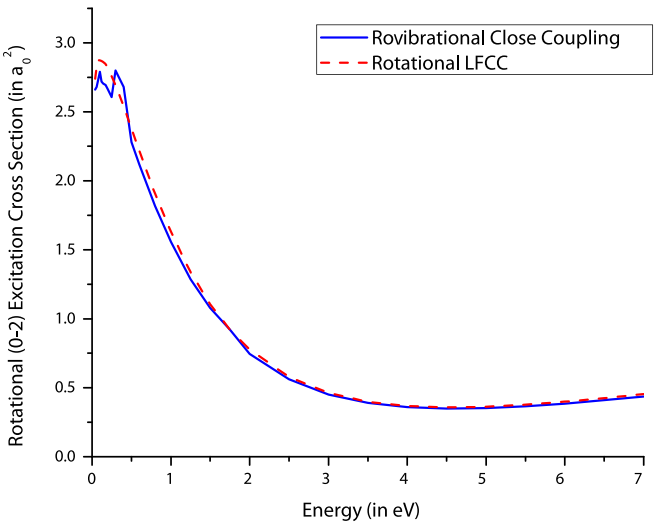

FIG. 16. Present computed angle-integrated rotational state-to-state $0 \rightarrow 2$ excitation cross section for vibrational elastic process in positron–carbon monoxide molecule collision.

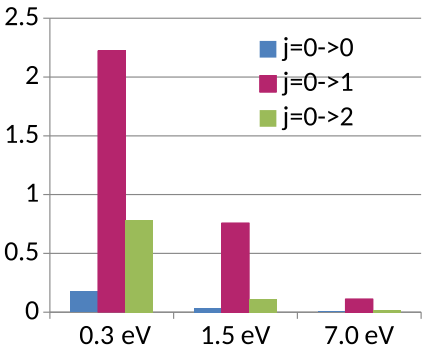

FIG. 17. Present computed angle-integrated rotational state-to-state elastic $0(j) \rightarrow 0(j')$, and excitation $0(j) \rightarrow 1(j')$ and $0(j) \rightarrow 2(j')$ cross sections for vibrational excitation $0(v) \rightarrow 1(v')$ excitation process (in a_0^2) for positron–carbon monoxide molecule collision.

state. In Fig. 17 we have plotted the rotational cross sections for the vibrational $0 \rightarrow 1$ excitation process. It is seen that for this vibrational excitation process the rotational $0 \rightarrow 1$ and $0 \rightarrow 2$ cross sections are higher than the rotational $0 \rightarrow 0$ cross section, unlike the results for the vibrational $0 \rightarrow 0$ process where the $0 \rightarrow 0$ cross sections are higher. Thus it is apparent that the probability of rotational transition from the ground rotational state ($j = 0$) for the vibrational ground state to the rotational states corresponding to excited vibrational states depends on the final vibrational state. In the present formalism this final-state effect is included through the vibrational coupling effect. All together we have found the importance of the rotational and vibrational coupling effect in positron-CO collision processes. However, to make any final comments on these, more theoretical and experimental works are necessary.

D. Vibrational and rotational energy transfer

Using Eq. (13) we have calculated the energy transfer using rovibrational and rotational LFCC methods. In Fig. 18 we have plotted those results (the rotational energy transfer is multiplied by 50) along with the results using the BFVCC method by Gianturco *et al.* The BFVCC results (multiplied by 50) for a positron–nitrogen molecule collision are also included in the figure for comparison. It is seen that the variation of the energy transfer with incident positron energy is the same calculated using different methods and for different molecules. The higher value of vibrational energy transfer using the rovibrational method is due to higher values of vibrational $0 \rightarrow 1$ excitation cross section compared to the BFVCC cross section, although the total cross section using BFVCC is higher than the result using the present rovibrational coupling scheme. The very low value of rotational energy transfer compared to that of vibrational energy transfer implies that the overall probability of transferring energy into the molecular rotational degrees of freedom is less than the molecular vibrational energy transfer. The higher value of vibrational energy transfer for CO when compared with the result of N_2 corresponds to higher efficiency of vibrational energy transfer for CO than N_2 which corroborates the observation that the CO molecule provides the environment for cooling of a hot positron more efficiently than N_2 as mentioned by Tenfen *et al.* [22].

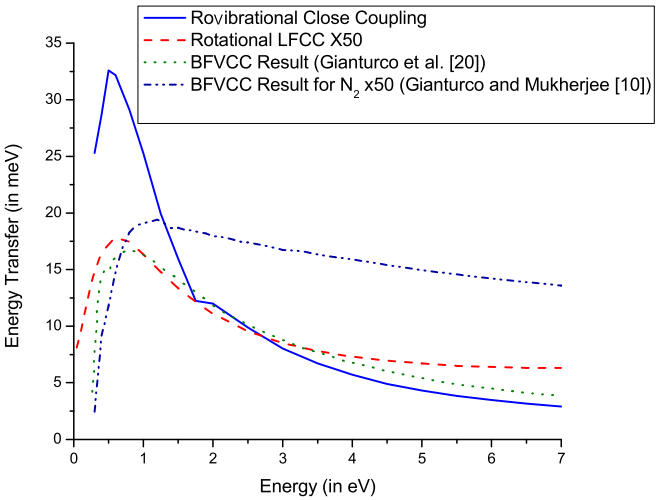

FIG. 18. Comparison between present computed average energy transfers as defined in Eq. (5) in the text using present rovibrational and rotational LFCC methods and BFVCC methods for positron–carbon monoxide molecule collision. The present rotational LFCC results are multiplied by 50. The BFVCC results for a nitrogen molecule by Gianturco and Mukherjee [10] (multiplied by 50) are also plotted for comparison.

III. CONCLUSION

In this work we have presented the calculated results for a positron–carbon monoxide collision using rovibrational close-coupling, rotational laboratory frame close-coupling (rotational LFCC), and LFCC adiabatic nuclei vibration (LFCC-ANV) methods. We have reported the angle-integrated rotationally elastic and state-to-state excitation, vibrational elastic and state-to-state excitation (summed over rotational), and total cross section (summed over vibrational and rotational) using the rovibrational close-coupling method. The rotational LFCC method is used to calculate the rotational and total cross sections (summed over rotational states). Using the LFCC-ANV method we have calculated the elastic and vibrational excitation cross sections. All the calculations are done using the positron correlation-polarization potential (PCOP) model to incorporate the correlation-polarization potential and the results are reported up to 7.0 eV. The results are compared with the theoretical results using the body fixed vibrational close-coupling (BFVCC) method performed by Gianturco *et al.* [20], the method of continued fractions (MCF) of Arretche *et al.* [21], and the multichannel MCF (MC-MCF) method of Tenfen *et al.* [22]. The present results are also compared with the measured values of Sullivan *et al.* [4], Kwan *et al.* [23], Sueoka and Hamada [24], and Zecca *et al.* [25]. In the first part of the discussions we have presented and compared some state-to-state potentials. It is seen that the natures of these potentials are different from those of homonuclear diatomic molecule like H_2 and N_2. In the next part of the discussions we have compared our computed total integrated cross sections (ICS) with the other theoretical and measured values. We have found some differences between the different theoretical values. It is to be noted that all the calculated data presented here are obtained using the same model PCOP correlation-polarization potential. Although the potentials are calculated using different electronic basis functions, the differences of the cross sections seem to not be so sensitive with the basis functions used. Thus the differences of the results may be attributed to the use of different coupling schemes. It is seen that the rotational coupling effect seems to be a very important contributor in determining the cross sections for positron-CO collision. To verify this we have also calculated the vibrational elastic cross sections (VECS) using the LFCC-ANV method and compared them with the results reported by Tenfen *et al.* [22]. The results also show the importance of the rotational coupling effect. The present results, when compared with the experimental data, show that the nature of the variation of the cross sections well agrees with the measured values. So far as the magnitude of the cross section is concerned, it is seen that the present rovibrational results match well with the measured values of Kwan *et al.* and Sueoka and Hamada. However, some differences have been observed with the results of Zecca *et al.* in the middle-energy region. The differences among all the theoretical results as well as the experimental data show the need for more theoretical and experimental works. We have also reported the vibrational and rotational inelastic cross sections. The vibrational $0 \rightarrow 1$ cross sections match well with the existing theories and the experimental results. However, the difference in the nature of the variation of this cross section with energy near the threshold also shows the effect of rotational dynamics in determination of the cross sections. The magnitudes of the vibrational $0 \rightarrow 2$ and $0 \rightarrow 3$ cross sections using rovibrational close coupling are found to be very small compared to $0 \rightarrow 1$ cross sections. These vibrational $0 \rightarrow 2$ and $0 \rightarrow 3$ cross sections using the rovibrational close-coupling scheme match well with the other theoretical calculations except the values calculated using the rotational LFCC-ANV method. Here we also have reported the computed rotational angle-integrated cross sections both for elastic and excitation processes. The plotted results show that the vibrational coupling effect has less influence on rotational cross sections in the vibrational elastic channel. However, the rotational cross sections corresponding to vibrational excitation channels show different behavior which represents the effect of vibrational coupling. Finally we have presented the computed vibrational and rotational energy transfer using rovibrational coupling and rotational LFCC methods, respectively. The results are also compared with the vibrational energy transfer for the N_2 molecule. The higher value of the present vibrational energy transfer compared to the present rotational energy transfer and the result for N_2 show that a positron cools down more efficiently in a CO molecule through transferring energy to vibrational excitation process. Additionally, we want to mention the work done by Machacek *et al.* [29] where they have presented the experimental cross sections on positron–hydrogen molecule collision in the large-energy region and compared their results with other experimental and theoretical results. They have found some differences among the theoretical and experimental results and attributed to the differences partially due to the exclusion of vibrational and rotational scattering from the calculations. Thus the present calculation on positron–carbon monoxide collision including rotational and vibrational motions of the molecule supports their observation on the importance of the inclusion of nuclear dynamics, at least for the lower-energy region.

[1] N. F. Lane, Rev. Mod. Phys. **52**, 29 (1980).
[2] A. S. Ghosh, N. C. Sil, and P. Mandal, Phys. Rep. **87**, 313 (1982).
[3] E. A. G. Armour, Phys. Rep. **169**, 1 (1988).
[4] J. P. Sullivan, S. J. Gilbert, and C. M. Surko, Phys. Rev. Lett. **86**, 1494 (2001).
[5] C. M. Surko, G. F. Gribakin, and S. J. Buckman, J. Phys. B: At., Mol. Opt. Phys. **38**, R57 (2005).
[6] W. Tenfen, K. T. Mazon, S. E. Michelin, and F. Arretche, Phys. Rev. A **86**, 042706 (2012).
[7] A. Jain, Phys. Rev. A **41**, 2437 (1990).
[8] M. Mukherjee, M. Basu, and A. S. Ghosh, J. Phys. B: At., Mol. Phys. **23**, 757 (1990).
[9] M. Mukherjee, T. Mukherjee, and A. S. Ghosh, J. Phys. B **24**, L463 (1991).
[10] F. A. Gianturco and T. Mukherjee, Phys. Rev. A **55**, 1044 (1997).
[11] T. Mukherjee and N. K. Sarkar, J. Phys. B: At., Mol. Phys. **41**, 125201 (2008).
[12] T. Mukherjee and M. Mukherjee, Phys. Rev. A **91**, 062706 (2015).
[13] M. Arthurs and A. Dalgarno, Proc. R. Soc. Lond. A **256**, 540 (1960).
[14] N. F. Lane and S. Geltman, Phys. Rev. **160**, 53 (1967).
[15] A. S. Ghosh and T. Mukherjee, Can. J. Phys. **74**, 420 (1996).
[16] K. T. Mazon, W. Tenfen, S. Michelin, F. Arretche, M.-T. Lee, and M. M. Fujimoto, Phys. Rev. A **82**, 032704 (2010).
[17] D. Assafrao, H. R. Walters, F. Arretche, A. Dutra, and J. R. Mohallem, Phys. Rev. A **84**, 022713 (2011).
[18] D. W. Norcross and N. T. Padial, Phys. Rev. A **25**, 226 (1982).
[19] A. S. Ghosh, T. Mukherjee, P. K. Biswas, and A. Jain, J. Phys. B: At., Mol. Phys. **26**, L23 (1993).
[20] F. A. Gianturco, T. Mukherjee, and P. Paioletti, Phys. Rev. A **56**, 3638 (1997).
[21] F. Arretche, K. T. Mazon, S. E. Michelin, M. M. Fujimoto, I. Iga, and M. T. Lee, Nucl. Instrum. Methods Phys. Res., Sect. B **266**, 441 (2008).
[22] W. Tenfen, F. Arretche, S. E. Michelin, and K. T. Mazon, Nucl. Instrum. Methods Phys. Res., Sect. B **362**, 25 (2015).
[23] C. K. Kwan, Y.-F. Hseih, W. E. Kauppila, S. J. Smith, T. S. Stein, M. N. Uddin, and M. S. Dababneh, Phys. Rev. A **27**, 1328 (1983).
[24] O. Sueoka and A. Hamada, J. Phys. Soc. Jpn. **62**, 2669 (1993).
[25] A. Zecca, L. Chiari, A. Sarkar, and M. Brunger, New J. Phys. **13**, 115001 (2011).
[26] A. D. McLean and M. Yoshimine, IBM J. Res. Dev. **12**, 206 (1967).
[27] Lu Peng-Fei, Yan Lei, Yu Zhong-Yuan, Gao Yu-Feng, and Gao Tao, Commun. Theor. Phys. **59**, 193 (2013).
[28] A. Jain, J. Phys. B: At., Mol. Phys. **19**, L105 (1986).
[29] J. R. Machacek, E. K. Anderson, C. Makochekanwa, S. J. Buckman, and J. Sullivan, Phys. Rev. A **88**, 042715 (2013).